

Action Functional as an Early Warning Indicator in the Space of Probability Measures via Schrödinger Bridge

Peng Zhang^{1,2,3,†}, Ting Gao^{1,2,3,5,*}, Jin Guo^{1,2,3,‡}, Jinqiao Duan^{4,3,5§}

¹ School of Mathematics and Statistics, Huazhong University of Science and Technology, China

² Center for Mathematical Science, Huazhong University of Science and Technology, China

³ Steklov-Wuhan Institute for Mathematical Exploration, Huazhong University of Science and Technology, China

⁴ Department of Mathematics and Department of Physics, Great Bay University, China

⁵ Guangdong Provincial Key Laboratory of Mathematical and Neural Dynamical Systems, Great Bay University, China.

Abstract

Critical transition and tipping phenomena between two meta-stable states in stochastic dynamical systems represents an important problem. In this work, we expand the methodology from the traditional Onsager-Machlup action functional, which typically identifies the most probable transition pathway between two meta-stable states, to investigate the evolutionary transition dynamics between two meta-stable invariant sets. To address this, we incorporate a comprehensive framework derived from Schrödinger bridge and Optimal Transport. In contrast to existing methodologies such as statistical analysis, bifurcation theory, information theory, statistical physics, topology, and graph theory for early warning indicators, we introduce a novel perspective on early warning signals within the realm of probability measures which enables the development of indicators grounded in action functionals.

In order to validate our framework, we apply this methodology to the Morris-Lecar model, which exhibits the generation of the repetitive firing in certain neurons resulting from a saddle-node bifurcation on an invariant circle. By varying the current condition, we investigate the transition dynamics between a meta-stable state and a stable invariant set (the limit cycle or homo-clinic orbit) within Morris-Lecar model. Additionally, we analyze real Alzheimer's data from the ADNI database to explore early warning signals indicating the transition from healthy to pre-AD states. This framework not only expands the transition pathway to encompass measures between two specified densities on invariant sets but also demonstrates potential of early warning indicators or biomarkers in complex diseases.

Keywords: Action functional; Schrödinger bridge; Early warning indicator; Transition dynamics; Morris-Lecar model; Alzheimer's Disease

1 Introduction

In the field of neuroscience, scientists have formulated hypotheses regarding the brain's critical dynamics, suggesting that the brain may exist in a state of phase transition between ordered and disordered activities. Some tipping points, at which the system becomes exceptionally vulnerable, could play a crucial role in the development of neural diseases. Consequently, a pivotal inquiry emerges: how does the critical brain hypothesis intersect with pathological conditions in contrast to normal brain function?

Transition pathway stands as a pivotal instrument in elucidating critical transitions or tipping phenomena within dynamical systems subject to intricate stochastic influences [1,2]. Strategies for the effective identification of transition pathways encompass a range of methodologies such as action functional theory [3–5], path integral methods [6], optimal transport, etc. Given the inherent complexity arising from the high dimensionality of real-world data with the intricate nature of invariant manifolds in dynamical systems, the Schrödinger bridge outstands as the optimal solution.

†Email: kazusa_zp@hust.edu.cn

*Email: tgao0716@hust.edu.cn

‡Email: jinguo0805@hust.edu.cn

§Email: duan@gbu.edu.cn

The Schrödinger bridge can be construed as a stochastic process aimed at identifying the optimal transition path measure in consideration of Brownian motion between two prescribed marginals. The Schrödinger bridge problem was originally introduced by Schrödinger [7] and can be construed as the optimal transport problem with entropy regularization. The study of the Schrödinger bridge problem is motivated by three main factors. Firstly, Schrödinger’s original thought experiment in statistical mechanics, addressing a large deviation problem rooted in quantum mechanics, serves as a foundational impetus. Secondly, the application of Sanov’s theorem [8] and Gibbs’s principle of conditioned reflection [9] facilitates the determination of the most probable Zustand-Verteilung (macrostate), akin to resolving a maximum entropy predicament. This scenario stands as an early and pivotal illustration of inference methodologies guiding the selection of a posterior distribution while minimizing assumptions beyond available data. The third motivation lies in perceiving these challenges as a means of regularizing the optimal mass transport (OMT) problem [10–14], thereby addressing its computational intricacies [15–17]. Indeed, the OMT problem represents the scenario in which the diffusion coefficient of Schrödinger bridge tends towards zero. Subsequently, significant efforts [18, 19] have been directed towards computing regularized OMT through algorithms of the Iterative Proportional Fitting (IPF) [20]-Fortet [21]-Sinkhorn [22] type.

Discovering a meaningful and computationally efficient approach to interpolate a high-dimensional probability distribution stands as a challenge of profound scientific importance, including generative modeling [23], transfer learning [24], cellular biology [25], etc. Currently, an increasing body of research leverages the Schrödinger bridge methodology to address this challenge. Pavon et al. [18] introduce an iterative procedure that employs constrained maximum likelihood estimation instead of nonlinear boundary couplings. They utilize importance sampling to propagate the functions ϕ and ψ in solving the Schrödinger system, drawing inspiration from Fortet-IPF-Sinkhorn type algorithms. Wang et al. [26] present a two-stage generative model employing entropy interpolation with the Schrödinger bridge. They develop their algorithm by incorporating the drift term, estimated by a deep score estimator and a deep density ratio estimator, into the Euler-Maruyama method. Bortoli et al. [27] introduce a novel framework that provides an approximation of the IPF method for addressing the Schrödinger bridge problem. This framework presents a computational tool for optimal transport, serving as a continuous state-space counterpart to the well-known Sinkhorn algorithm. Chen et al. [28] establish a computationally feasible Schrödinger bridge connecting paired data by introducing a versatile reference stochastic differential equation. This approach enables the generation of mel-spectrograms from latent representations of clean text. Chen et al. [29] present a computational framework for likelihood training of Schrödinger bridge models, which is the most similar method to ours. Drawing from the theory of forward-backward stochastic differential equations, they transform the optimality conditions of Schrödinger bridge into a system of stochastic differential equations, facilitating efficient model training. By leveraging Schrödinger bridge theory, these methods enhance the efficiency of computing transition measures between distributions to a certain degree.

Various dynamical systems, spanning ecosystems [30], climate [31, 32], economic structures [33] and social frameworks [34, 35] can manifest a tipping point, triggering a complete system collapse [36, 37]. Forecasting these tipping points represents a significant and exceedingly arduous challenge. Recent examples garnering significant interest involve neurodegenerative disorders, such as Alzheimer’s disease (AD) [38]. Numerous studies [39, 40] have been undertaken to identify the change point marking the onset of accelerated atrophy in AD. These investigations have revealed that the rate of brain atrophy in AD does not exhibit a linear progression but rather undergoes a gradual acceleration several years prior to the manifestation of symptoms [41]. Simons et al. [38] proposes that tipping points and their associated elements could offer a valuable concept for enhancing the comprehension of AD. Tipping points, aligning with the concept that minor alterations at a specific juncture can yield substantial and enduring repercussions within a system, encapsulating the idea that small changes can yield significant outcomes. The detection of early warning signals which imminent critical transitions is crucial, given the substantial challenges involved in reverting a system to its previous state following such events [42, 43]. The phenomenon of critical slowing down underpins various effective indicators in Early Warning Systems (EWS), encompassing heightened autocorrelation [37], variance [44, 45], and higher-order moments such as skewness and kurtosis [46] of the system’s response amplitude distribution, which fluctuate as the system approaches a critical point. These metrics are derived from data employing a sliding window technique. The relevant quantiles are assessed within a window comprising multiple data points in the time series, sliding forward at a suitable time increment to capture temporal variations. Certain scenarios exist where transitions occur without preceding critical slowing down [47, 48]. Subsequent studies tackle this constraint by employing multivariate data analysis to assess false alarms [49], incorporating metrics such as link density [50], clustering coefficient [51], characteristic path length [52], etc. Other studies detect early warning signals through dynamic changes of the network structure [53, 54] and from inconsistency of predictions and the fluctuation of

hidden state representations [55, 56]. In contrast to these methods, we aim to identify suitable indicators within the realm of probability measures, as certain rare events are more readily detectable within the framework of probability space.

In summary, the goal of this study is to model and analyze transition dynamics, including brain activity, to detect early warnings of abrupt changes within these systems. Our main contributions are

- **Early Warning Indicator:** Define an action functional, i.e. the Wasserstein distance in Benamou-Brenier representation, as early warning indicator in probability measure space.
- **Transition Pathway between Invariant Manifolds:** Develop an efficient way to detect transition paths between two compact invariant manifolds.
- **Validation:** Validate our method on real Alzheimer’s Disease Neuroimaging Initiative (ADNI) data and Morris-Lecar neuron model which describes a variety of oscillatory voltage patterns of Barnacle muscle fibers under different current.

The rest of this paper is organized as follows: Section 2 provides a review of the foundational concepts of the Schrödinger bridge and its equivalent formulations. Subsequently, we introduce a novel tipping indicator in probability space, derived from the action functional of the path measure of the Schrödinger bridge. In Section 4, we validate our framework through numerical experiments using real ADNI data. Lastly, our conclusion is presented in Section 5.

2 Background knowledge on Schrödinger bridge

The most probable stochastic evolution between two prescribed marginal distributions ρ_0 and ρ_1 corresponds to the solution of the Schrödinger bridge problem:

$$\mathcal{P}_{SB} := \operatorname{argmin}\{D_{KL}(P\|W) | P \in \mathcal{D}(\rho_0, \rho_1)\} \quad (1)$$

where \mathcal{D} is the space of probability measures on $\Omega = C([0, 1], X)$, and $W \in M_+(\Omega)$ is the reference path measure on Ω . Here X is a complete connected Riemannian manifold without boundary, $M_+(\Omega)$ denotes positive measures on Ω .

Consider the Schrödinger bridge problem with prior reference measure \bar{W} , which has the canonical coordinate process

$$dX_t = f(t, X_t)dt + \sigma_t d\bar{W}_t \quad (2)$$

where f is the drift term and σ_t denotes the noisy density. The optimal control formulation can be written as [57]

$$\begin{cases} \min_{u \in \mathcal{U}} \mathcal{J}(u) = \mathbb{E} \left[\int_0^1 \frac{1}{2\sigma_t^2} \|u_t\|^2 dt \right], & (3) \\ dX_t = [f(t, X_t) + u_t]dt + \sigma_t d\bar{W}_t, & (4) \\ X_0 \sim \rho_0(x), X_1 \sim \rho_1(y), & (5) \end{cases}$$

where the family \mathcal{U} consists of adapted, finite-energy control functions.

Next, we present several versions of equivalent for Schrödinger bridge problem.

2.1 Coupled partial differential equations with boundary conditions

Let $(\varphi, \hat{\varphi})$ be the solution of the following coupled partial differential equations (PDE)

$$\frac{\partial \varphi_t}{\partial t} + f \cdot \nabla \varphi_t + \frac{\sigma_t^2}{2} \Delta \varphi_t = 0, \quad (6)$$

$$\frac{\partial \hat{\varphi}_t}{\partial t} + \nabla \cdot (f \hat{\varphi}_t) - \frac{\sigma_t^2}{2} \Delta \hat{\varphi}_t = 0 \quad (7)$$

with boundary conditions

$$\varphi(0, x) \cdot \hat{\varphi}(0, x) = \rho_0(x), \quad (8)$$

$$\varphi(1, y) \cdot \hat{\varphi}(1, y) = \rho_1(y). \quad (9)$$

Moreover, the solution can be expressed by the path measure of the following forward stochastic differential equations (SDE)

$$dX_t = (f(t, X_t) + \sigma_t^2 \nabla_x \ln \varphi(t, X_t)) dt + \sigma_t dW_t, \quad X_0 \sim \rho_0, \quad (10)$$

and the backward SDE

$$dX_t = (f(t, X_t) - \sigma_t^2 \nabla_x \ln \hat{\varphi}(t, X_t)) dt + \sigma_t dW_t, \quad X_1 \sim \rho_1. \quad (11)$$

2.2 Relationship between Benamou-Brenier problem and Schrödinger bridge

The dynamic version of the OMT problem was already accomplished by Benamou and Brenier [15] by

$$\begin{aligned} \mathcal{W}_2(\rho_0, \rho_1) &= \inf_{(\mu, v)} \int_0^1 \int_{\mathbb{R}^n} \|v(t, x)\|^2 \mu_t(dx) dt, \\ \frac{\partial \mu_t}{\partial t} + \nabla \cdot (v \mu_t) &= 0, \\ \mu_0 &= \rho_0, \quad \mu_1 = \rho_1. \end{aligned} \quad (12)$$

The fluid-dynamic formulation for the Schrödinger bridge can be derived as [58] the problem

$$\begin{aligned} \inf_{(\rho, v)} \int_{\mathbb{R}^n} \int_0^1 \left[\frac{1}{2} \|v(t, x)\|^2 + \frac{\sigma_t^2}{8} \|\nabla \log \rho\|^2 \right] \rho(t, x) dt dx \\ \frac{\partial \rho}{\partial t} + \nabla \cdot (v \rho) &= 0, \\ \rho(0, x) &= \rho_0(x), \quad \rho(1, y) = \rho_1(y). \end{aligned} \quad (13)$$

The fluid-dynamic formulation (13) could be viewed as regularizations of the Benamou-Brenier problem (12). As $\sigma_t \rightarrow 0$, the solution to problem (13) converges to the solution of the Benamou-Brenier problem (12) [15]. By variable substitution, the fluid-dynamic formulation (13) is equivalent to

$$\begin{aligned} \inf_{(\rho, v)} \int_{\mathbb{R}^n} \int_0^1 \left[\frac{1}{2} \|v(t, x)\|^2 \right] \rho(t, x) dt dx \\ \frac{\partial \rho}{\partial t} + \nabla \cdot (v \rho) - \frac{\sigma_t^2}{2} \Delta \rho &= 0, \\ \rho(0, x) &= \rho_0(x), \quad \rho(1, y) = \rho_1(y). \end{aligned} \quad (14)$$

2.3 Forward and backward generators

Denote $R \in M_+(\Omega)$ as a Markov measure, its forward stochastic derivative $\partial + \overrightarrow{L}^W$ is defined by

$$\left[\partial_t + \overrightarrow{L}_t^W \right] (u)(t, x) := \lim_{h \downarrow 0} h^{-1} \mathbb{E}_W (u(t+h, X_{t+h}) - u(t, X_t) \mid X_t = x) \quad (15)$$

for any measurable function $u : [0, 1] \times \mathcal{X} \rightarrow \mathbb{R}$ in the set $\text{dom } \overrightarrow{L}^W$ for which the limit exists $W_t - a.e.$ for all $0 \leq t < 1$. Since the time reversed W^* of W is still Markov, W admits a backward stochastic derivative $-\partial + \overleftarrow{L}^W$ which is defined by

$$\left[-\partial_t + \overleftarrow{L}_t^W \right] u(t, x) := \lim_{h \downarrow 0} h^{-1} \mathbb{E}_W (u(t-h, X_{t-h}) - u(t, X_t) \mid X_t = x) \quad (16)$$

for any measurable function $u : [0, 1] \times \mathcal{X} \leftarrow \mathbb{W}$ in the set $\text{dom } \overleftarrow{L}^W$ for which the limit exists $W_t - a.e.$ for all $0 < t \leq 1$.

Denote $\overrightarrow{L}^W = \overleftarrow{L}^W = L$ without the superscript W and without the time arrows, since W is assumed to be reversible.

To give the expressions of the generators \overrightarrow{A} and \overleftarrow{A} , we should introduce the carré du champ of W as

$$\Gamma(u, v) := L(uv) - uLv - vLu \quad (17)$$

Algorithm 1: Likelihood training of SB-FBSDE

Input: boundary distributions p_{data} and p_{prior} , parameterized policies $Z(\cdot, \cdot; \theta)$ and $\hat{Z}(\cdot, \cdot; \phi)$

- 1 **for** $k = 1$ **to** K **do**
- 2 Sample $X_{t \in [0, T]}$ from (19), where $x_0 \sim p_{\text{data}}$ (computational graph retained);
- 3 compute \mathcal{L} with (22);
- 4 Update (θ, ϕ) with $\nabla_{\theta, \phi} \mathcal{L}_{SB}(x_0; \theta, \phi)$
- 5 **end**

In general, the forward and backward generators $(\partial_t + \overrightarrow{A}_t)_{0 \leq t \leq 1}$ and $(-\partial_t + \overleftarrow{A}_t)_{0 \leq t \leq 1}$ of P depend explicitly on t .

Under some hypotheses in [13] on measure W , the forward and backward generators of P are given for any function $u : [0, 1] \times \mathcal{X} \rightarrow \mathbb{R}$ belonging to some class \mathcal{U} of regular functions, by

$$\begin{cases} \overrightarrow{A}_t u(x) = Lu(x) + \frac{\Gamma(\varphi_t, u)(x)}{\varphi_t(x)}, & (t, x) \in [0, 1] \times \mathcal{X} \\ \overleftarrow{A}_t u(x) = Lu(x) + \frac{\Gamma(\hat{\varphi}_t, u)(x)}{\hat{\varphi}_t(x)}, & (t, x) \in (0, 1] \times \mathcal{X} \end{cases} \quad (18)$$

where $\varphi_t, \hat{\varphi}_t$ are defined by

$$\begin{cases} \varphi_t(z) := \mathbb{E}_W(\varphi_0(X_0) \mid X_t = z) \\ \hat{\varphi}_t(z) := \mathbb{E}_W(\hat{\varphi}_1(X_1) \mid X_t = z) \end{cases}, \quad \text{for } P_t\text{-a.e. } z \in \mathcal{X}.$$

Rigorous statement and proof are given in [59].

2.4 Forward-backward stochastic differential equations

By nonlinear Feynman-Kac formulation [60], the Schrödinger bridge problem can be derived as the following forward-backward SDEs representation [29]

$$\begin{cases} dX_t = (f + \sigma_t^2 \nabla \ln \varphi_t) dt + \sigma_t dW_t & (19) \\ dY_t = \frac{1}{2} \sigma_t^2 (\nabla \ln \varphi_t)^2 dt + \sigma_t \nabla \ln \varphi_t dW_t & (20) \\ d\hat{Y}_t = (\frac{1}{2} \sigma_t^2 (\nabla \ln \hat{\varphi}_t)^2 + \nabla_x \cdot (\sigma_t^2 \nabla \ln \hat{\varphi}_t - f) + \sigma_t^2 \nabla \ln \hat{\varphi}_t \nabla \ln \varphi_t) dt + \sigma_t \nabla \ln \hat{\varphi}_t dW_t & (21) \end{cases}$$

with boundary conditions $X_0 = x_0, x_0 \sim \rho_0$ and $Y_1 + \hat{Y}_1 = \ln \rho_1(X_1)$. Here (19) and (20,21) respectively represent the forward and backward SDEs.

In the following example, we employ Chen et al. [29] as our computational framework for finding the optimal transition path measure in forward-backward SDE. The loss function is defined by the log-likelihood of the Schrödinger bridge problem as

$$\mathcal{L} = -\ln p_0(x_0) = \int_0^1 \mathbb{E} \left[\frac{1}{2} (\|\sigma_t \nabla \varphi_t\|^2 + \|\sigma_t \nabla \hat{\varphi}_t\|^2) + \nabla_x \cdot (\sigma_t^2 \nabla \hat{\varphi}_t - f) \right] dt - \mathbb{E}[\ln p_1(X_1)], \quad (22)$$

where the expectation is taken over the forward SDE (19) with the initial condition $X_0 = x_0$. The training details are shown in Alg. 1.

2.5 Equivalence between Onsager-Machlup action functional and Schrödinger bridge

One of the ways to characterize the most probable transition pathway of a stochastic process between two metastable states is the Onsager-Machlup action functional. This scenario can be viewed as a specific instance of identifying the most probable transition path between two specified marginal distributions, i.e. two Dirac delta distributions. Huang et al. [61] prove the equivalence between the Onsager-Machlup action functional and the corresponding Markovian bridge process. They refer

$$dY_t = [f(Y_t) + \sigma_t^2 \nabla \log p(x_T, T | Y_t, t)] dt + \sigma_t dW_t, \quad t \in [0, T] \quad (23)$$

as the bridge SDE associated with Eq.(2). This equation is originally derived by Doob [62] from the probabilistic perspective via the Doob *h-transform* of SDE (2). The relationship between most probable transition pathway and Markovian bridges is shown in [61] (Theorem 3.9) as follows:

Theorem 2.1. Suppose that the assumptions $\mathcal{H}.1$ and $\mathcal{H}.2$ in [61] hold.

(i). The most probable transition path of the system (2) coincides with the most probable transition path of the associated bridge SDE (23).

(ii). A path $\psi^* \in C_{x_0, x_T}^2[0, T]$ is the most probable transition path of (2) if and only if it solves the following first-order ODE

$$d\psi^*(t) = [f(\psi^*(t)) + \sigma_t^2 \nabla \ln p(x_T, T | \psi^*(t), t)] dt, \quad t \in (0, T), \quad \psi^*(0) = x_0,$$

where $p(\cdot, \cdot | \cdot, \cdot)$ is the transition density of the solution process of (2), and $C_{x_0, x_T}^2[0, T]$ denotes the space of all continuous \mathbb{R}^k -valued curves on time interval $[0, T]$ connecting x_0 and x_T .

3 Tipping indicator in probability space

Sudden transitions to a different state, once a threshold is passed, is known as tipping. Tipping point refers the critical point in a situation, process, or system beyond which a significant and often unstoppable effect or change takes place. Tipping points commonly signify instances where a system undergoes abrupt, swift, and occasionally irreversible transformations. Mathematically, a tipping point is regarded as a critical state connecting the states before and after the bifurcation in a complex dynamical system. However, the general concept of the tipping point is not only limited to the transition through a bifurcation point, but it could also be related to the abrupt transition caused by instantaneously internal switches of structures or/and alterations of internal parameters. Ashwin et al. [31] identify three mechanisms of tipping: bifurcation-induced, noise-induced, and rate-induced tipping.

Warning signals for critical transitions hold significant importance due to the considerable challenges involved in restoring a system to its previous state post such transitions [42, 63, 64]. Various early warning indicators could be formulated with methods in statistics, bifurcation theory, information theory, statistical physics, topology, graph theory and so on [65–67]. Besides, in climate dynamics [68], various regions in the world have been classified as tipping elements as they are considered to be under the threat of a critical transition. The definitions of "tipping elements" here inspires us to give the following definition of critical transition and tipping indicator in probability space.

Definition 3.1. (Tipping in probability space) A tipping point in probability space exists if there exists a control parameter ρ with a critical value ρ_c , at which a small parameter variation ($\delta\rho > 0$) leads to a qualitative change C in our tipping indicator, i.e.,

$$|I(\delta\rho + \rho_c) - I(\rho_c)| \geq C.$$

This definition of action functional in probability measure space is actually easy to interpolate from a geometric point of view, since it has been shown that certain types of PDEs whose solution are flow of probability measures, are gradient flows with respect to the Wasserstein metric. In [69], a cost function which is a perturbed version of the Wasserstein cost \mathcal{W}_2 is introduced to define that for any regular function on the set of probability measures.

It is also interesting to associate Lagrangian with this. Here we denote our indicator as the action functional defined on the optimal path measure via Schrödinger bridge. Then we get

$$\mathcal{W}_2(\rho_0, \rho_1) = \inf_{(\nu, \rho)} \int_0^1 \int_{\mathbb{R}^n} \|\nu(t, x)\|^2 \rho_t(dx) dt. \quad (24)$$

where $\nu(t, x)$ is a smooth vector field. That is the cost in fluid formulation (14). Therefore, denoting μ_t^* as the optimal path measure, we have the time-dependent early warning indicator defined as:

$$I(\rho_t^*) = \frac{1}{t} \inf_{(\nu, \rho)} \int_0^t \int_{\mathbb{R}^n} \|\nu(t, x)\|^2 \rho_t(dx) dt. \quad (25)$$

4 Experiments

4.1 Morris-Lecar model

The Morris-Lecar model is a simplified two-dimensional biophysical model of action potential generation proposed by Catherine Morris and Harold Lecar [70]. This model exhibits the generation of the repetitive firing

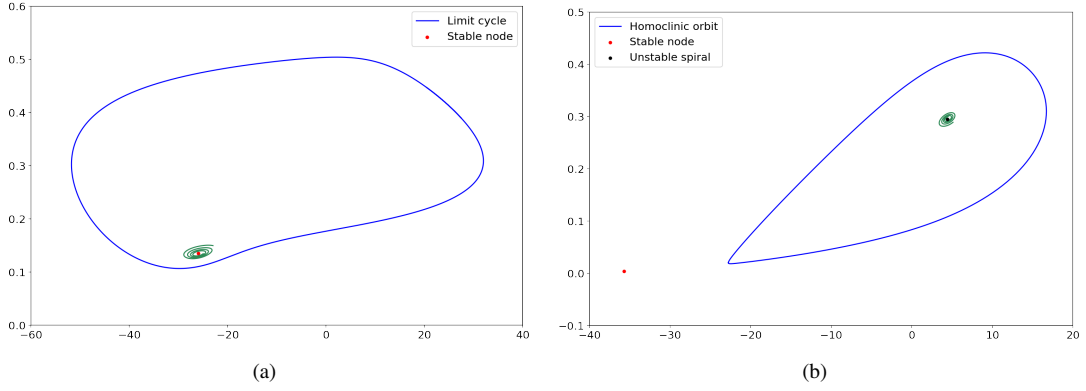


Figure 1: (a) The stable node and stable limit cycle of the Morris-Lecar model with bifurcation parameter $I = 92 \mu A/cm^2$. (b) The stable node, unstable spiral and stable homoclinic cycle of the Morris-Lecar model with bifurcation parameter $I = 37 \mu A/cm^2$.

in certain neurons results from a saddle-node bifurcation on an invariant circle. The model has three channels: potassium ion channel, calcium ion channel and leakage current channel. The model is represented as follows

$$\begin{cases} dv_t = \frac{1}{C} [-g_{Ca}m_\infty(v_t)(v_t - V_{Ca}) - g_K w_t(v_t - V_K) - g_L(v_t - V_L) + I] dt + \sigma_t dW_t, & (26) \\ dw_t = \phi \frac{w_\infty(v_t) - w_t}{\tau_w(v_t)} dt, & (27) \end{cases}$$

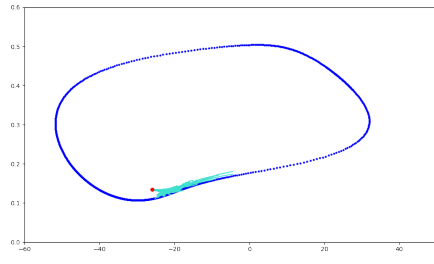
where

$$\begin{aligned} m_\infty(v) &= 0.5 \left[1 + \tanh\left(\frac{v - V_1}{V_2}\right) \right], \\ w_\infty(v) &= 0.5 \left[1 + \tanh\left(\frac{v - V_3}{V_4}\right) \right], \\ \tau_w(v) &= \left[\cosh\left(\frac{v - V_3}{2V_4}\right) \right]^{-1} \end{aligned}$$

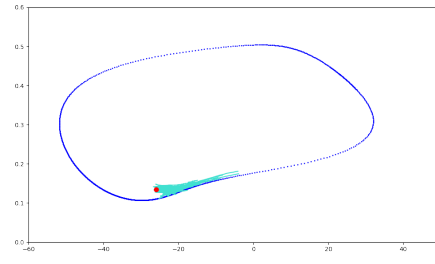
Here, W_t is a Brownian motion, and σ_t is the nonnegative noise intensity. The variable v_t represents the membrane potential, and $w_t \in [0, 1]$ represents the activation variable of potassium ion, reflecting the evolution of the opening probability of potassium ion channels. The parameters g_{Ca} , g_K and g_L are the maximum conductances of calcium channel, potassium channel and leakage current channel, respectively. The V_{Ca} , V_K and V_L are the reversal potentials of the above channels, respectively. The parameter I represents the impressed input current from the environment, and m_∞ and w_∞ are the steady-state values of the opening probability Ca^{2+} channel and K^+ channel, respectively. Parameter C is the membrane capacitance, and ϕ represents the change between the fast and slow scales of the neuron. V_1 , V_2 , V_3 , and V_4 are the parameters selected for the clamp data.

Figure 1(a) shows two invariant sets of the Morris-Lecar model under Class I parameters, which is a bistable system for some parameters, with a unique stable equilibrium and a stable limit cycle. In addition, it is worth noting that there are also unstable periodic solutions (the small limiting period in Figure 1(a)). The trajectory separates these initial conditions approaching the stable fixed point from those approaching the large stable limit cycle. The stable limit cycle corresponds to the continuous oscillation state of the neuronal system described by the Morris-Lecar model, while the unique fixed point corresponds to the resting state of the neuronal system. Figure 1(b) shows three invariant sets of the Morris-Lecar model, with a stable node, a unstable spiral and a stable limit cycle under Class II parameters. The parameter details are outlined in Table 1 in Appendix A.

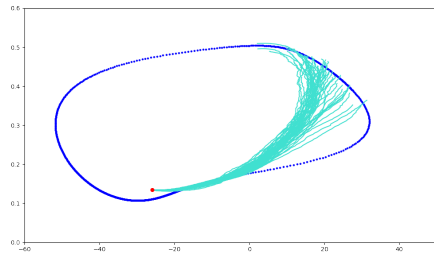
In a theoretical framework, we could endeavor to simulate the transition dynamics by aiming for an invariant measure on the stable limit cycle as the terminal time approaches infinity. Achieving precise simulation outcomes necessitates sufficiently small time steps and a large terminal time, ensuring that accumulated errors remain within acceptable bounds. Failure to adhere to these requirements may result in the approximation of the target set being limited to a subset of the entire limit cycle. However, the exigency of retaining all intermediate results incurs a considerable computational cost, leading to memory constraints. Consequently, given the computational resources, we confine the target set to a subset of the limit cycle.



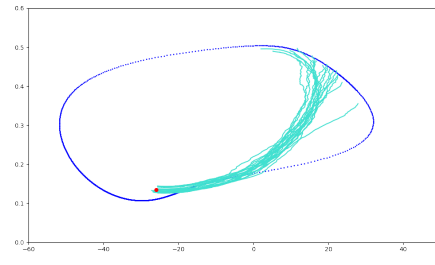
(a) $T=20, N=200, g=0.3$, forward.



(b) $T=20, N=200, g=0.3$, backward.



(c) $T=20, N=200, g=0.5$, forward.



(d) $T=20, N=200, g=0.5$, backward.

Figure 2: Transition path dynamics between a stable state and invariant manifold in Morris-Lecar system. Upper row: evolutionary pathways when terminal time $T = 20$ and noise strength $g = 0.3$, from forward SDE (Left) and backward SDE (Right). Bottom row: evolutionary pathways when time $T = 20$ and noise strength $g = 0.5$, from forward SDE (Left) and evolutionary pathways from backward SDE (Right).

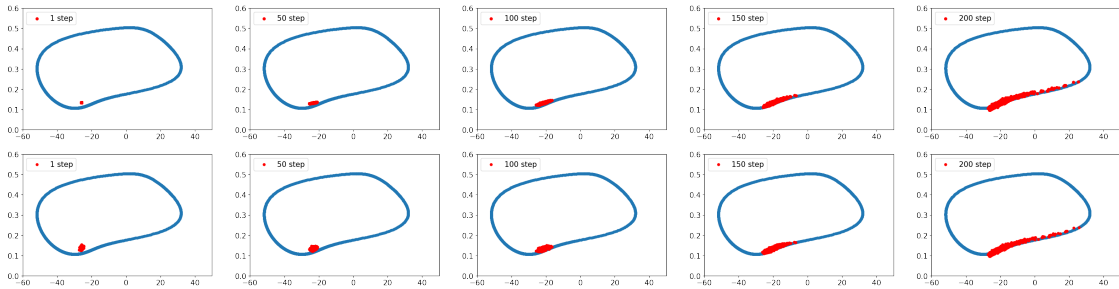


Figure 3: The evolutionary density of transition paths from the stable node to the stable limit cycle with $T=20, N=200, g=0.3$.

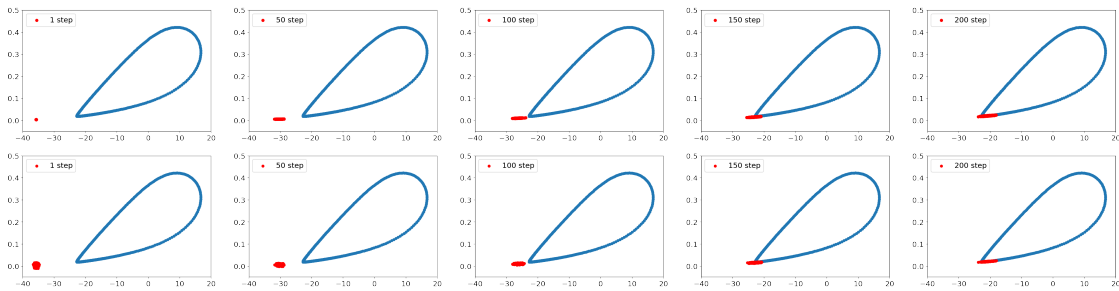


Figure 4: The evolutionary density of transition paths from the stable node to the stable homoclinic cycle with $T=20, N=200, g=0.3$.

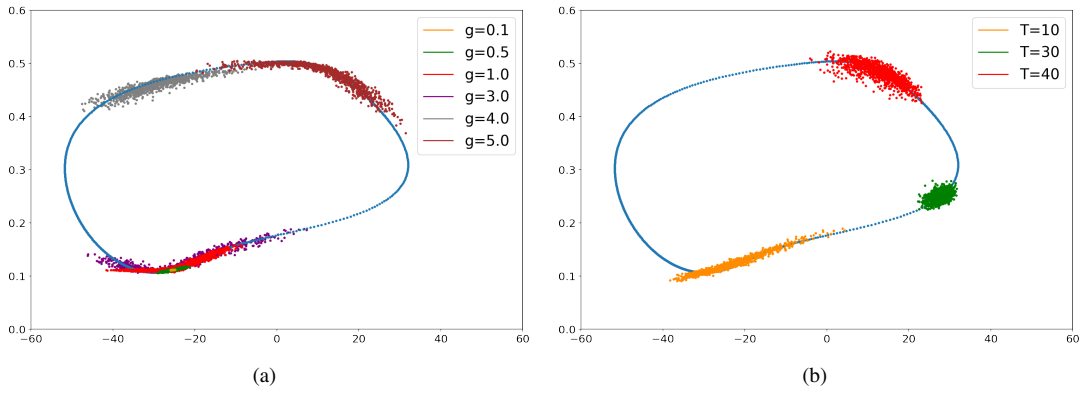


Figure 5: Terminal density concentrations of the transition from the stable node to the stable limit cycle, with (a) $T = 3$ under various noise density g . (b) $g = 1$ under various terminal time T .

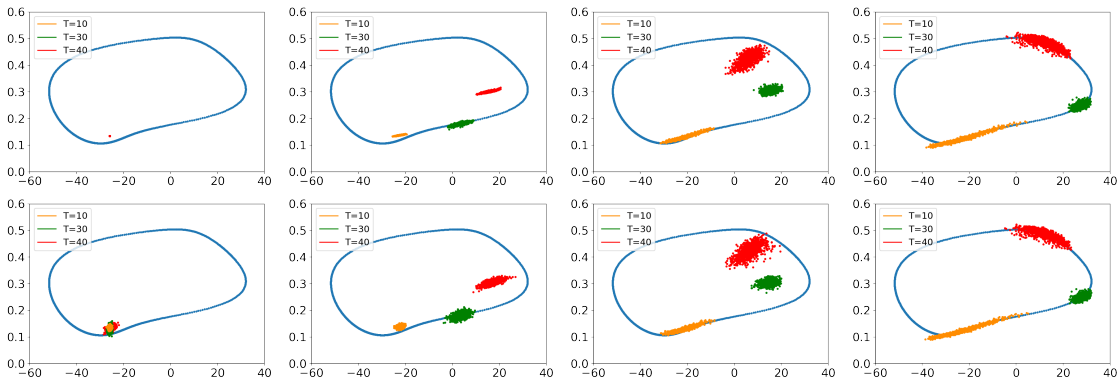


Figure 6: The evolutionary densities of transition paths dynamics over time for various terminal time $T = 10, 30$ and 40 .

Figure 2 shows the transition paths dynamics between the stable equilibrium and the invariant manifold, i.e. the limit cycle. We can see that as the noise increases, the transition paths will reach the target area with further distances. We can also see the terminal time effect of different T values. Figure 3 and Figure 4 shows the time evolutionary density of transition paths from the stable node to the stable limit cycle or the stable homoclinic cycle. The consistency of evolutionary density patterns between the forward and backward pathways means the convergence of our numerical solution to the Schrödinger bridge problem.

Figure 5(a) and Figure 5(b) show the terminal density concentrations of the transition from the stable node to the stable limit cycle with various noise and terminal time. Figure 6 presents the evolutionary densities of transition paths dynamics over time for various terminal time $T = 10, 30$ and 40 . For more detail effects of the noise strength, please see Figure 11 in Appendix B.

4.2 Alzheimer's disease neuroimage

AD is distinguished by a progressive and seemingly continuous pathological progression, marked by the development of neurodegeneration exhibiting distinct spatial and temporal dynamics. Specific characteristics can strongly indicate the diagnosis of AD. In AD, the brain typically exhibits at least moderate cortical atrophy, particularly pronounced in multimodal association cortices and limbic lobe structures. Structural neuroimaging with MRI can be employed to evaluate atrophy as a metric of neurodegeneration in AD. We conduct our experiment on dataset originates from <https://www.kaggle.com/datasets/kaushalsethia/alzheimers-adni> (Samples in Figure 7(a)).

Researchers [71] have determined that the presence of abnormally tangled tau proteins serves as a sign of numerous instances of Alzheimer's disease. They noted that the tau protein undergoes a crucial *tipping point* transition, shifting from a healthy to a pathological state. Upon crossing this tipping point, tangles are rapidly formed. Once this threshold is surpassed, the brain transitions into the irreversible clinical phase, losing

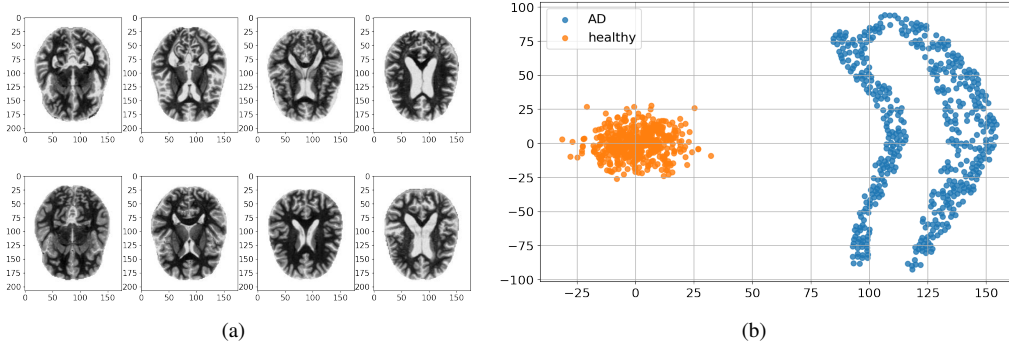


Figure 7: (a) Sample ADNI data for mild disease brain (first row) and healthy brain (second row). (b) T-SNE representation of healthy samples (orange color) and illness samples (blue color).

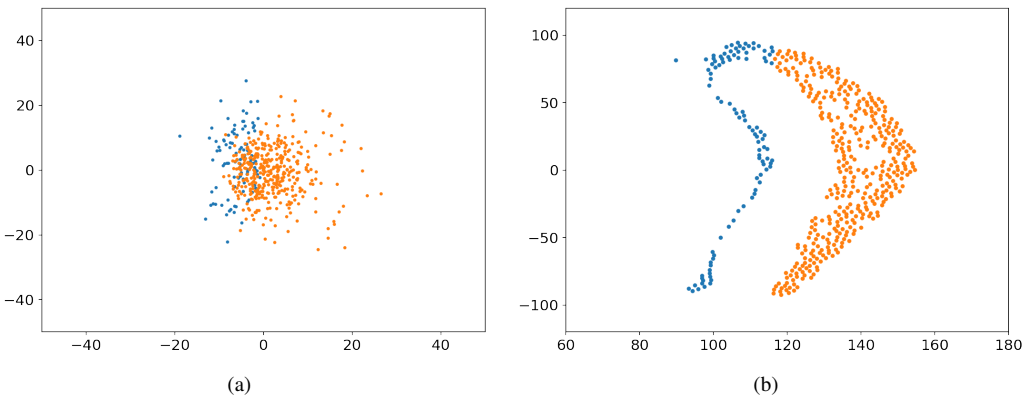


Figure 8: After optimal unit decomposition, (a) initial distribution; (b) target distribution.

opportunities for intervention [38]. Therefore, the detection of the tipping point in Alzheimer’s disease holds significant importance, enabling medical professionals to intervene effectively before the onset of the clinical phase.

Due to the difficulty of detecting the tipping point in high-dimensional time series, we need to reduce the dimension of brain MRI data to the plane. Firstly, the Variational AutoEncoder (VAE) [72] model is employed to extract features from the representation space, educing the image data to 20-dimensional vectors. Subsequently, these 20-dimensional vectors are projected into a 2-dimensional space utilizing the t-distributed Stochastic Neighbor Embedding (t-SNE) [73] method. The following is the visualization of healthy and AD patients after VAE and t-SNE reduction (Figure 7(b)).

By observing Figure 7(b), it becomes evident that the data pertaining to early-stage mild cognitive impairment exhibits a non-convex configuration post dimensionality reduction. According to Brenier’s Theorem ([74, 75]), any transport map can be decomposed into a measure preserving map and a solution to the Monge-Ampère equation. Therefore, under the L^2 cost function, the regularity of solution to the Monge-Ampère equation determines the continuity of the transport map. If the support set characterizing the target distribution lacks connectivity or convexity, the optimal transport map will manifest discontinuous property. Nonetheless, conventional neural networks are confined to approximate continuous mappings, thus engendering inherent conflicts that precipitate convergence challenges and the phenomenon of pattern collapse. To redress this quandary, we embrace the methodology delineated in [76, 77], predicated upon the discrete Brenier theory to approximate the continuous Brenier potential.

Specifically, denote the initial measure as μ over the convex compact domain Ω , and the objective measure ν as an empirical measure, i.e. $\nu = \sum_{i=1}^n \nu_i \delta(y - y_i)$, where $Y = \{y_1, y_2, \dots, y_n\}$, and ν_i meet $\sum_{i=1}^n \nu_i = \mu(\Omega)$. Each training sample y_i corresponds to the support plane of the Brenier potential energy function, denoted by

$$\pi_{h,i}(x) := \langle x, y_i \rangle + h_i,$$

and the height vector is defined as $h = (h_1, h_2, \dots, h_n)$. Denote $\omega_i(h) = \mu(W_i(h)) = \int_{W_i(h) \cap \Omega} d\mu$, by

Algorithm 2: Training process for ADNI data

Input: boundary distributions p_{data} and $p_{\text{prior}} = \sum_{i=1}^n v_i \delta(y - y_i)$, parameterized policies $Z(\cdot, \cdot; \theta)$ and $\hat{Z}(\cdot, \cdot; \phi)$, number of Monte Carlo samples N , positive integer s .

- 1 Initialize $h = (h_1, h_2, \dots, h_n) \leftarrow (0, 0, \dots, 0)$.
- 2 **while** $E(h)$ has not decreased for s steps **do**
- 3 Generate N uniformly distributed samples from $\{x_j\}_{j=1}^N$.
- 4 Calculate $\nabla h = (\hat{w}_i(h) - v_i)^T$.
- 5 $\nabla h = \nabla h - \text{mean}(\nabla h)$.
- 6 Update h .
- 7 **end**
- 8 **for** $k = 1$ to K **do**
- 9 Sample $X_{t \in [0, T]}$ from (19), where $x_0 \sim p_{\text{data}}$ (computational graph retained);
- 10 compute \mathcal{L} with (28);
- 11 Update (θ, ϕ) with $\nabla_{\theta, \phi} \mathcal{L}_{SB}(x_0; \theta, \phi)$
- 12 **end**

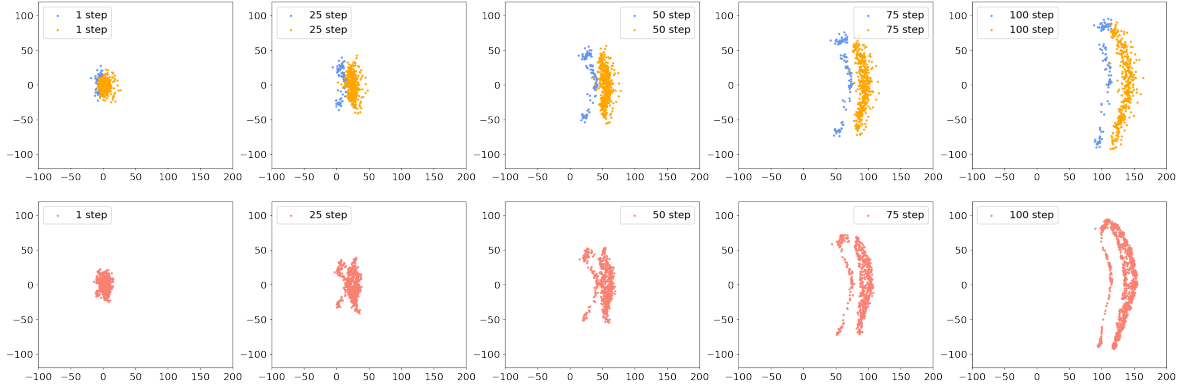


Figure 9: The evolutionary density from healthy state to early Alzheimer's state.

semi-discrete Optimal Transport Map [77], the vector h is the unique minimizer of the energy $E(h) = \int_0^h \sum_{i=1}^n \omega_i(\eta) d\eta_i - \sum_{i=1}^n h_i v_i$.

The figure of the Brenier potential function is a convex polyhedron with each support plane $\pi_{h,i}(x)$ corresponding to one of the faces of the polyhedron. Under a semi-discrete transport map $T : \Omega \rightarrow Y$, a cell decomposition is induced $\Omega = \cup_{i=1}^n W_i$, such that every x in each cell W_i is mapped to the target y_i , $T : x \in W_i \rightarrow y_i$. The map T is measure preserving, denoted as $T_{\#}\mu = \nu$, if the transport map satisfies $T(W_i) = y_i$ and $\mu(W_i) = v_i$. The specific training process is shown in algorithm 2.

By McCann interpolation, the target distribution satisfies $\rho_1(x_1) = (\nabla\varphi)_{\#}\rho_0(x_0)$, where φ is the Kantorovich potential. Under L^2 cost function, the Brenier theory indicates that the optimal transport T and Kantorovich potential φ meets $T(x) = Id(x) - \nabla\varphi(x)$. Furthermore, we obtain $T(x) = \nabla(\pi_{h,i}(x)) = y_i$. Therefore, the $\rho_1(x_1) = (\nabla\varphi)_{\#}\rho_0(x_0) = (Id - T)_{\#}\rho_0(x_0)$. Then we modify the loss function (22) into

$$\mathcal{L} = -\ln p_0(x_0) = \int_0^1 \mathbb{E} \left[\frac{1}{2} (\|\sigma_t \nabla \varphi_t\| + \|\sigma_t \nabla \hat{\varphi}_t\|)^2 + \nabla_x \cdot (\sigma_t^2 \nabla \hat{\varphi}_t - f) \right] dt - \mathbb{E}[(x_1 - y_i)^2], \quad (28)$$

where $x_0 \in W_i$, and x_1 is the propagated terminal state which starts from x_0 by forward SDE (19).

Due to the non-convex geometric shape of target data, we divide it into two connected regions, as the blue part and orange part in Figure (8(b)). Then by Semi-discrete Optimal Transport Map, we obtain the corresponding two parts in initial data, which is shown in Figure (8(a)). Next, we propagate the FBSDEs for the two parts respectively. The algorithm is shown in Algorithm 2.

We employed reduced MRI images from 1100 healthy individuals as the initial distribution and from 750 AD patients as the target distribution. The pathway dynamics from the initial to the target distribution are established via the Schrödinger bridge theory, which could be viewed as an entropy-regularized optimal transport problem.

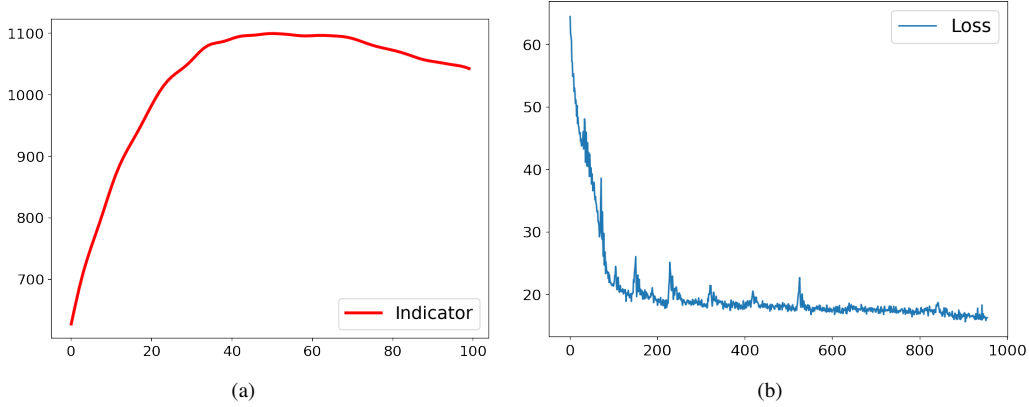


Figure 10: (a) The action functional indicator defined in Eq.(25). (b) Loss over iterations.

To identify the tipping point from the healthy brain state to the AD brain state, we compute the estimates of $\nabla \ln \phi_t$ and density ρ_t via the loss function described in Eq.(22).

The embedding densities of the two datasets can now be employed to compare tipping phenomena. We choose terminal time $T = 1$, $N = 100$ and the noise intensity g is adaptive to time change [78]. From Figure 9, we can see the time evolutionary density from healthy state to Alzheimer state. The consistent evolution of the first and second rows across steps in Figure 9 represents that the determined density involution converges, a theoretical guarantee provided by [13,79]. It's obvious that the geometric of samples undergoes a sudden change around the 25-th step, aligning with the abrupt tipping indicated by our defined indicator in (25). That implies that a critical transition in the brain state occurs around 25-th step, emphasizing the need for intervention prior to the tipping point.

Figure 10(a) illustrates the temporal consistency of the most probable density change over time. This trajectory represents the optimal transition path between the two sets via Schrödinger bridge, which is guaranteed to be convergent based on the forward-backward SDE with the loss function in Figure 10(b), as well as the forward and backward consistency in Figure 9.

5 Conclusion

In this paper, we introduce a novel and effective method for automatically detecting abnormalities in neural images. Our approach leverages Schrödinger bridge with early warning indicators which facilitate us in two aspects. On the one hand, we investigate the transition path dynamics in terms of path measures between two meta-stable invariant sets. On the other hand, we study the early warning signals of real ADNI data via action functional in probability space. The ability to identify transitions between meta-stable states plays a pivotal role in predicting and controlling brain behavior and functionality. We here find that action functional indicator in probability space a good metric to measure the sudden discrepancy as density changes over time.

There are still many challenging problems need to be solved in the future. For example, as the geometric representation of images on low dimensional manifold can greatly affect the convergence of our algorithm, one important direction is to develop better algorithms considering geometric properties of the given densities.

Acknowledgements

This work was supported by the National Key Research and Development Program of China (No. 2021ZD0201300), the National Natural Science Foundation of China (No. 12141107), the Fundamental Research Funds for the Central Universities (5003011053), the Guangdong-Dongguan Joint Research Grant 2023A151514 0016, and is partly supported by the Guangdong Provincial Key Laboratory of Mathematical and Neural Dynamical Systems.

Data availability

The data that support the findings of this study are openly available upon request.

A Parameters for Morri-Lecar Model

The parameter details outlined in Section 4.1 are presented in Table 1. In the table, the second column corresponds to a scenario featuring one stable state and a stable cycle, while the third column corresponds to a situation with a stable node, an unstable spiral, and a stable limit cycle.

Table 1: The parameters for Morri-Lecar model.

Parameter	Class I (Hopf)	Class II (Homoclinic)
g_{Ca}	4.4	4
g_K	8	8
g_L	2	2
E_{Ca}	120	120
E_K	-84	-84
E_L	-60	-60
I	92	37
C	20	20
ϕ	0.04	0.23
V_1	-1.2	-1.2
V_2	18	18
V_3	2	12
V_4	30	17.4

B Transition Paths Dynamics over Time

References

- [1] Jinqiao Duan. *An introduction to stochastic dynamics*, volume 51. Cambridge University Press, 2015.
- [2] Ting Gao and Jinqiao Duan. Stochastic dynamics and data science. *Stochastics and Dynamics*, page 2340002, 2023.
- [3] Wei Wei, Ting Gao, Xiaoli Chen, and Jinqiao Duan. An optimal control method to compute the most likely transition path for stochastic dynamical systems with jumps. *Chaos: An Interdisciplinary Journal of Nonlinear Science*, 32(5), 2022.
- [4] Jianyu Chen, Ting Gao, Yang Li, and Jinqiao Duan. Detecting the most probable high dimensional transition pathway based on optimal control theory. *arXiv preprint arXiv:2303.00385*, 2023.
- [5] Jin Guo, Ting Gao, Peng Zhang, Jiequn Han, and Jinqiao Duan. Deep reinforcement learning in finite-horizon to explore the most probable transition pathway. *Physica D: Nonlinear Phenomena*, 458:133955, 2024.
- [6] Yuanfei Huang, Ying Chao, Wei Wei, and Jinqiao Duan. Estimating the most probable transition time for stochastic dynamical systems. *Nonlinearity*, 34(7):4543, 2021.
- [7] Erwin Schrödinger. Sur la théorie relativiste de l'électron et l'interprétation de la mécanique quantique. In *Annales de l'institut Henri Poincaré*, volume 2, pages 269–310, 1932.
- [8] Ivan Nicolaevich Sanov. On the probability of large deviations of random variables. *Selected Translations in Mathematical Statistics and Probability*, 1:213–244, 1961.
- [9] Amir Dembo. *Large deviations techniques and applications*. Springer, 2009.
- [10] Guillaume Carlier, Vincent Duval, Gabriel Peyré, and Bernhard Schmitzer. Convergence of entropic schemes for optimal transport and gradient flows. *SIAM Journal on Mathematical Analysis*, 49(2):1385–1418, 2017.

- [11] Simone Di Marino and Augusto Gerolin. An optimal transport approach for the schrödinger bridge problem and convergence of sinkhorn algorithm. *Journal of Scientific Computing*, 85(2):27, 2020.
- [12] Christian Léonard. From the schrödinger problem to the monge–kantorovich problem. *Journal of Functional Analysis*, 262(4):1879–1920, 2012.
- [13] Christian Léonard. A survey of the schrödinger problem and some of its connections with optimal transport. *arXiv preprint arXiv:1308.0215*, 2013.
- [14] Toshio Mikami and Michele Thieullen. Optimal transportation problem by stochastic optimal control. *SIAM Journal on Control and Optimization*, 47(3):1127–1139, 2008.
- [15] Jean-David Benamou and Yann Brenier. A computational fluid mechanics solution to the monge–kantorovich mass transfer problem. *Numerische Mathematik*, 84(3):375–393, 2000.
- [16] Sigurd Angenent, Steven Haker, and Allen Tannenbaum. Minimizing flows for the monge–kantorovich problem. *SIAM journal on mathematical analysis*, 35(1):61–97, 2003.
- [17] Nikita Gushchin, Alexander Kolesov, Petr Mokrov, Polina Karpikova, Andrei Spiridonov, Evgeny Burnaev, and Alexander Korotin. Building the bridge of schrödinger: A continuous entropic optimal transport benchmark. *Advances in Neural Information Processing Systems*, 36, 2024.
- [18] Michele Pavon, Giulio Trigila, and Esteban G Tabak. The data-driven schrödinger bridge. *Communications on Pure and Applied Mathematics*, 74(7):1545–1573, 2021.
- [19] Espen Bernton, Jeremy Heng, Arnaud Doucet, and Pierre E Jacob. Schrödinger bridge samplers. *arXiv preprint arXiv:1912.13170*, 2019.
- [20] W Edwards Deming and Frederick F Stephan. On a least squares adjustment of a sampled frequency table when the expected marginal totals are known. *The Annals of Mathematical Statistics*, 11(4):427–444, 1940.
- [21] Robert Fortet. Résolution d’un système d’équations de m. schrödinger. *Journal de Mathématiques Pures et Appliquées*, 19(1-4):83–105, 1940.
- [22] Richard Sinkhorn. A relationship between arbitrary positive matrices and doubly stochastic matrices. *The annals of mathematical statistics*, 35(2):876–879, 1964.
- [23] Martin Arjovsky, Soumith Chintala, and Léon Bottou. Wasserstein generative adversarial networks. In *International conference on machine learning*, pages 214–223. PMLR, 2017.
- [24] Behnam Neyshabur, Hanie Sedghi, and Chiyuan Zhang. What is being transferred in transfer learning? *Advances in neural information processing systems*, 33:512–523, 2020.
- [25] Geoffrey Schiebinger, Jian Shu, Marcin Tabaka, Brian Cleary, Vidya Subramanian, Aryeh Solomon, Joshua Gould, Siyan Liu, Stacie Lin, Peter Berube, et al. Optimal-transport analysis of single-cell gene expression identifies developmental trajectories in reprogramming. *Cell*, 176(4):928–943, 2019.
- [26] Gefei Wang, Yuling Jiao, Qian Xu, Yang Wang, and Can Yang. Deep generative learning via schrödinger bridge. In *International conference on machine learning*, pages 10794–10804. PMLR, 2021.
- [27] Valentin De Bortoli, James Thornton, Jeremy Heng, and Arnaud Doucet. Diffusion schrödinger bridge with applications to score-based generative modeling. *Advances in Neural Information Processing Systems*, 34:17695–17709, 2021.
- [28] Zehua Chen, Guande He, Kaiwen Zheng, Xu Tan, and Jun Zhu. Schrodinger bridges beat diffusion models on text-to-speech synthesis. *arXiv preprint arXiv:2312.03491*, 2023.
- [29] Tianrong Chen, Guan-Horng Liu, and Evangelos A Theodorou. Likelihood training of schrödinger bridge using forward-backward sdes theory. *arXiv preprint arXiv:2110.11291*, 2021.
- [30] Jason M Tylianakis and Camille Coux. Tipping points in ecological networks. *Trends in plant science*, 19(5):281–283, 2014.

- [31] Peter Ashwin, Sebastian Wieczorek, Renato Vitolo, and Peter Cox. Tipping points in open systems: bifurcation, noise-induced and rate-dependent examples in the climate system. *Philosophical Transactions of the Royal Society A: Mathematical, Physical and Engineering Sciences*, 370(1962):1166–1184, 2012.
- [32] Jeremy T Kerr, Alana Pindar, Paul Galpern, Laurence Packer, Simon G Potts, Stuart M Roberts, Pierre Rasmont, Oliver Schweiger, Sheila R Colla, Leif L Richardson, et al. Climate change impacts on bumblebees converge across continents. *Science*, 349(6244):177–180, 2015.
- [33] Stanislao Gualdi, Marco Tarzia, Francesco Zamponi, and Jean-Philippe Bouchaud. Tipping points in macroeconomic agent-based models. *Journal of Economic Dynamics and Control*, 50:29–61, 2015.
- [34] Vasilis Dakos and Jordi Bascompte. Critical slowing down as early warning for the onset of collapse in mutualistic communities. *Proceedings of the National Academy of Sciences*, 111(49):17546–17551, 2014.
- [35] Lei Dai, Daan Vorselen, Kirill S Korolev, and Jeff Gore. Generic indicators for loss of resilience before a tipping point leading to population collapse. *Science*, 336(6085):1175–1177, 2012.
- [36] Malcolm Gladwell. *The tipping point: How little things can make a big difference*. Little, Brown, 2006.
- [37] Marten Scheffer, Jordi Bascompte, William A Brock, Victor Brovkin, Stephen R Carpenter, Vasilis Dakos, Hermann Held, Egbert H Van Nes, Max Rietkerk, and George Sugihara. Early-warning signals for critical transitions. *Nature*, 461(7260):53–59, 2009.
- [38] Mikael Simons, Johannes Levin, and Martin Dichgans. Tipping points in neurodegeneration. *Neuron*, 111(19):2954–2968, 2023.
- [39] William Jagust. Imaging the evolution and pathophysiology of alzheimer disease. *Nature Reviews Neuroscience*, 19(11):687–700, 2018.
- [40] Basil H Ridha, Josephine Barnes, Jonathan W Bartlett, Alison Godbolt, Tracey Pepple, Martin N Rossor, and Nick C Fox. Tracking atrophy progression in familial alzheimer’s disease: a serial mri study. *The Lancet Neurology*, 5(10):828–834, 2006.
- [41] Kirsi M Kinnunen, David M Cash, Teresa Poole, Chris Frost, Tammie LS Benzinger, R Laila Ahsan, Kelvin K Leung, M Jorge Cardoso, Marc Modat, Ian B Malone, et al. Presymptomatic atrophy in autosomal dominant alzheimer’s disease: a serial magnetic resonance imaging study. *Alzheimer’s & dementia*, 14(1):43–53, 2018.
- [42] Carl Folke, Steve Carpenter, Brian Walker, Marten Scheffer, Thomas Elmqvist, Lance Gunderson, and Crawford Stanley Holling. Regime shifts, resilience, and biodiversity in ecosystem management. *Annu. Rev. Ecol. Evol. Syst.*, 35:557–581, 2004.
- [43] Marten Scheffer, Steve Carpenter, Jonathan A Foley, Carl Folke, and Brian Walker. Catastrophic shifts in ecosystems. *Nature*, 413(6856):591–596, 2001.
- [44] Matias I Maturana, Christian Meisel, Katrina Dell, Philippa J Karoly, Wendyl D’Souza, David B Grayden, Anthony N Burkitt, Premysl Jiruska, Jan Kudlacek, Jaroslav Hlinka, et al. Critical slowing down as a biomarker for seizure susceptibility. *Nature communications*, 11(1):2172, 2020.
- [45] Niklas Boers. Early-warning signals for dansgaard-oeschger events in a high-resolution ice core record. *Nature communications*, 9(1):2556, 2018.
- [46] Daniel B Wright and Joshua A Herrington. Problematic standard errors and confidence intervals for skewness and kurtosis. *Behavior research methods*, 43:8–17, 2011.
- [47] Maarten C Boerlijst, Thomas Oudman, and André M de Roos. Catastrophic collapse can occur without early warning: examples of silent catastrophes in structured ecological models. *PloS one*, 8(4):e62033, 2013.
- [48] Carl Boettiger, Noam Ross, and Alan Hastings. Early warning signals: the charted and uncharted territories. *Theoretical ecology*, 6:255–264, 2013.

- [49] Richard Streeter and Andrew J Dugmore. Anticipating land surface change. *Proceedings of the National Academy of Sciences*, 110(15):5779–5784, 2013.
- [50] Xueli Yang, Zhi-Hua Wang, and Chenghao Wang. Critical transitions in the hydrological system: early-warning signals and network analysis. *Hydrology and Earth System Sciences*, 26(7):1845–1856, 2022.
- [51] Mirjam Van Der Mheen, Henk A Dijkstra, Avi Gozolchiani, Matthijs Den Toom, Qingyi Feng, Juergen Kurths, and Emilio Hernandez-Garcia. Interaction network based early warning indicators for the atlantic moc collapse. *Geophysical Research Letters*, 40(11):2714–2719, 2013.
- [52] V Godavarthi, VR Unni, EA Gopalakrishnan, and RI Sujith. Recurrence networks to study dynamical transitions in a turbulent combustor. *Chaos: An Interdisciplinary Journal of Nonlinear Science*, 27(6), 2017.
- [53] Rui Liu, Jiayuan Zhong, Renhao Hong, Ely Chen, Kazuyuki Aihara, Pei Chen, and Luonan Chen. Predicting local covid-19 outbreaks and infectious disease epidemics based on landscape network entropy. *Science Bulletin*, 66(22):2265–2270, 2021.
- [54] Jiayuan Zhong, Chongyin Han, Yangkai Wang, Pei Chen, and Rui Liu. Identifying the critical state of complex biological systems by the directed-network rank score method. *Bioinformatics*, 38(24):5398–5405, 2022.
- [55] Yuyan Tong, Renhao Hong, Ze Zhang, Kazuyuki Aihara, Pei Chen, Rui Liu, and Luonan Chen. Earthquake alerting based on spatial geodetic data by spatiotemporal information transformation learning. *Proceedings of the National Academy of Sciences*, 120(37):e2302275120, 2023.
- [56] Pei Chen, Rui Liu, Kazuyuki Aihara, and Luonan Chen. Autoreservoir computing for multistep ahead prediction based on the spatiotemporal information transformation. *Nature communications*, 11(1):4568, 2020.
- [57] Yongxin Chen, Tryphon T Georgiou, and Michele Pavon. Stochastic control liaisons: Richard sinkhorn meets gaspard monge on a schrodinger bridge. *Siam Review*, 63(2):249–313, 2021.
- [58] Yongxin Chen, Tryphon T Georgiou, and Michele Pavon. On the relation between optimal transport and schrödinger bridges: A stochastic control viewpoint. *Journal of Optimization Theory and Applications*, 169:671–691, 2016.
- [59] Christian Léonard. Stochastic derivatives and generalized h-transforms of markov processes, 2011.
- [60] Ioannis Exarchos and Evangelos A Theodorou. Stochastic optimal control via forward and backward stochastic differential equations and importance sampling. *Automatica*, 87:159–165, 2018.
- [61] Yuanfei Huang, Qiao Huang, and Jinqiao Duan. The most probable transition paths of stochastic dynamical systems: a sufficient and necessary characterisation. *Nonlinearity*, 37(1):015010, 2023.
- [62] Joseph L Doob. Conditional brownian motion and the boundary limits of harmonic functions. *Bulletin de la Société Mathématique de France*, 85:431–458, 1957.
- [63] Lingyu Feng, Ting Gao, Wang Xiao, and Jinqiao Duan. Early warning indicators via latent stochastic dynamical systems. *Chaos: An Interdisciplinary Journal of Nonlinear Science*, 34(3), 2024.
- [64] Peng Zhang, Ting Gao, Jin Guo, Jinqiao Duan, and Sergey Nikolenko. Early warning prediction with automatic labeling in epilepsy patients, 2024.
- [65] Marina Hirota, Milena Holmgren, Egbert H Van Nes, and Marten Scheffer. Global resilience of tropical forest and savanna to critical transitions. *Science*, 334(6053):232–235, 2011.
- [66] Rong Wang, John A Dearing, Peter G Langdon, Enlou Zhang, Xiangdong Yang, Vasilis Dakos, and Marten Scheffer. Flickering gives early warning signals of a critical transition to a eutrophic lake state. *Nature*, 492(7429):419–422, 2012.
- [67] Thomas Quail, Alvin Shrier, and Leon Glass. Predicting the onset of period-doubling bifurcations in noisy cardiac systems. *Proceedings of the National Academy of Sciences*, 112(30):9358–9363, 2015.

- [68] Timothy M. Lenton, Hermann Held, Elmar Kriegler, Jim W Hall, Wolfgang Lucht, Stefan Rahmstorf, and Hans Joachim Schellnhuber. Tipping elements in the earth’s climate system. *Proceedings of the National Academy of Sciences*, 105:1786 – 1793, 2008.
- [69] Ivan Gentil, Christian Léonard, and Luigia Ripani. Dynamical aspects of the generalized schrödinger problem via otto calculus—a heuristic point of view. *Revista matemática iberoamericana*, 36(4):1071–1112, 2020.
- [70] Catherine Morris and Harold Lecar. Voltage oscillations in the barnacle giant muscle fiber. *Biophysical journal*, 35(1):193–213, 1981.
- [71] Eloise Masquelier, Esther Taxon, Sheng-Ping Liang, Yahya Al Sabeh, Lior Sepunaru, Michael J Gordon, and Daniel E Morse. A new electrochemical method that mimics phosphorylation of the core tau peptide k18 enables kinetic and structural analysis of intermediates and assembly. *Journal of Biological Chemistry*, 299(3), 2023.
- [72] Diederik P Kingma and Max Welling. Auto-encoding variational bayes. *arXiv preprint arXiv:1312.6114*, 2013.
- [73] Laurens Van der Maaten and Geoffrey Hinton. Visualizing data using t-sne. *Journal of machine learning research*, 9(11), 2008.
- [74] Yann Brenier. Polar decomposition and increasing rearrangement of vector-fields. *COMPTEs RENDUS DE L ACADEMIE DES SCIENCES SERIE I-MATHEMATIQUE*, 305(19):805–808, 1987.
- [75] Yann Brenier. Polar factorization and monotone rearrangement of vector-valued functions. *Communications on pure and applied mathematics*, 44(4):375–417, 1991.
- [76] Dongsheng An, Yang Guo, Na Lei, Zhongxuan Luo, Shing-Tung Yau, and Xianfeng Gu. Ae-ot: A new generative model based on extended semi-discrete optimal transport. *ICLR 2020*, 2019.
- [77] Na Lei, Yang Guo, Dongsheng An, Xin Qi, Zhongxuan Luo, Shing-Tung Yau, and Xianfeng Gu. Mode collapse and regularity of optimal transportation maps. *arXiv preprint arXiv:1902.02934*, 2019.
- [78] Alexander Quinn Nichol and Prafulla Dhariwal. Improved denoising diffusion probabilistic models. In *International conference on machine learning*, pages 8162–8171. PMLR, 2021.
- [79] Michael S Albergo, Nicholas M Boffi, and Eric Vanden-Eijnden. Stochastic interpolants: A unifying framework for flows and diffusions. *arXiv preprint arXiv:2303.08797*, 2023.

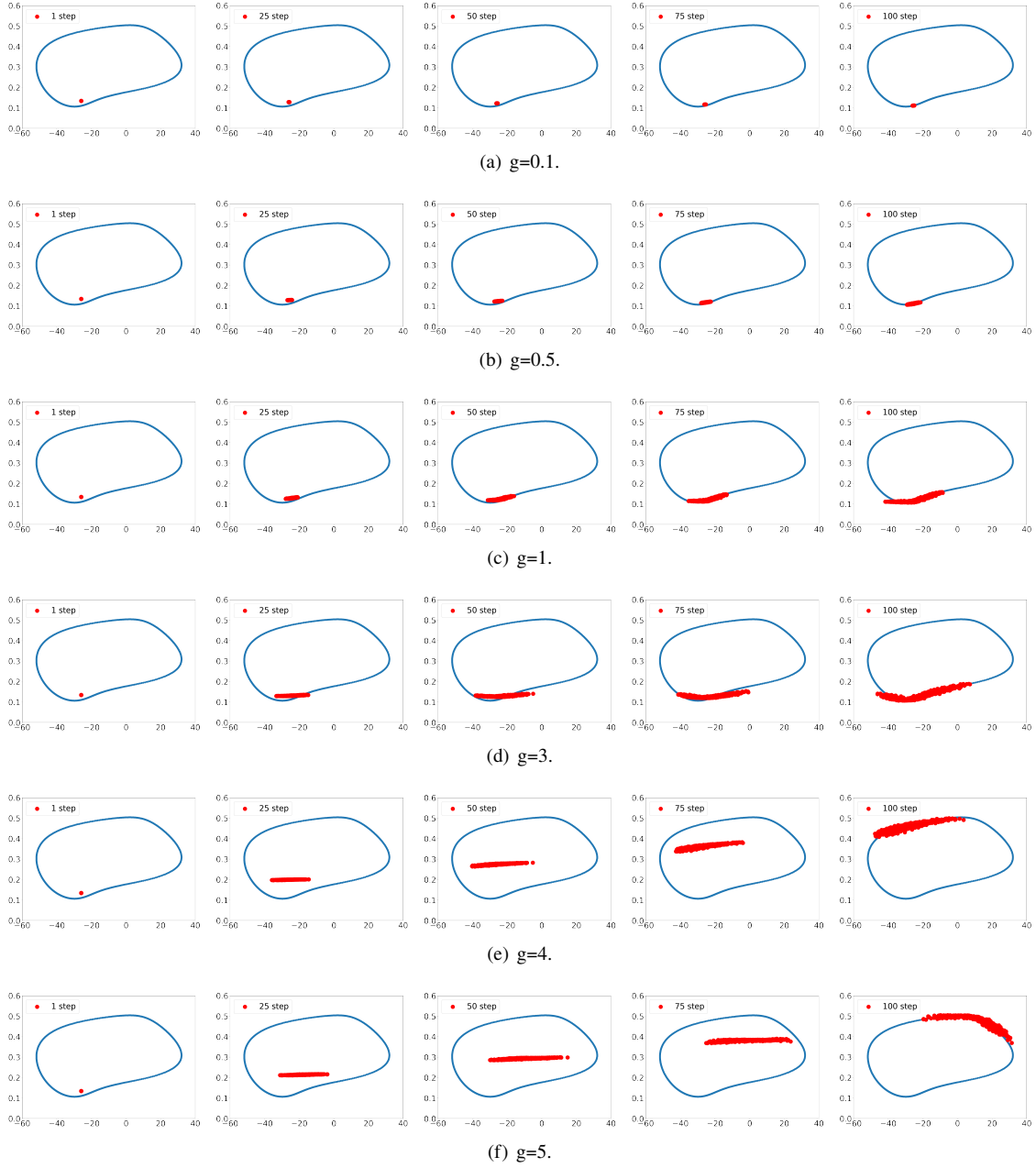


Figure 11: The evolutionary densities of transition paths dynamics over time for various noise density g .